An Experimental Study of the Signal to Noise Ratio of Radiated Emissions in the Presence of Thermal Noise in a Reverberation Chamber

Andrew C. Marvin
Department of Electronic Engineering
University of York
York, UK
andy.marvin@york.ac.uk

Simon J. Bale
Department of Electronic Engineering
University of York
York, UK
simon.bale@york.ac.uk

***Abstract*—In this paper the phenomenon of thermal noise present in a reverberation chamber and received through an antenna within the chamber is reviewed. The consequences of the thermal noise are described in terms of the observed signal to noise ratio of a signal radiated by an equipment-under-test placed at a number of positions in the chamber. It is shown that the observed signal-to-noise ratio is dependent on both the position of the equipment-under-test within the chamber and on the stirrer position.**

Keywords—reverberation chamber, antenna noise temperature, signal to noise ratio.

I. INTRODUCTION

The use of reverberation chambers for the measurement of the total power radiated by an equipment-under-test (EUT) is well established and described in the IEC Standard 61000-4-21 [1]. Little attention has been paid to the issues associated with the measurement of low-level signals radiated by EUTs in the presence of the noise originating in the receiver system and the thermal noise originating from the reverberation chamber itself. The minimum observable signal is limited by the total noise at the receiver input which is the sum of the equivalent input noise of the receiver and the thermal noise received by the antenna originating from within the chamber. The properties of this thermal noise are described in [2]. In this paper we review the thermal noise properties of the reverberation chamber and present experiment data showing how the signal-to-noise ratio of a received signal from an EUT in the chamber depends on both the position of the EUT in the chamber and the position of the rotating stirrer. Potential applications of this work include aspects of signal security.

In Section II the thermal noise properties of a reverberation chamber are reviewed, the measurement system used in the experiments is described in Section III, and the measured results are presented in Section IV.

II. PROPERTIES OF THERMAL NOISE IN A REVERBERATION CHAMBER

Any antenna receives thermal noise from its surroundings. This noise power can be described in terms of an antenna noise temperature T_{ANT} such that the noise power available from the antenna under conjugate impedance matched conditions is P_{ANT}.

$$P_{ANT} = kT_{ANT}B \tag{1}$$

In (1), k is Boltzmann's constant and B is the observation bandwidth. If the antenna is installed in an anechoic chamber with assumed perfect absorbers, then T_{ANT} is the ambient temperature of the chamber absorber. The antenna noise can be represented as a Thévenin series voltage source embedded in the real part of the antenna output impedance. For an antenna installed in a reverberation chamber the situation is more complex. Whilst the chamber wall and stirrer surfaces are highly reflective, they are not perfectly reflective. This imperfection contributes energy losses contributing in part to the finite chamber Q-factor [3]. These resistive losses have associated thermal (Nyquist) noise which radiates into the chamber to be received by the antenna. It is shown in [2] that the apparent antenna noise temperature of an antenna installed in a reverberation chamber is dependent on the position of the rotating mechanical stirrer as follows. The antenna has an input reflection coefficient which can be measured on a 50 Ω impedance vector network analyser (VNA) as $S11_{ANT}$ for each stirrer position. The antenna feeds a receiver system with an input reflection coefficient measured as $S11_{sys}$. The two reflection coefficients have a resulting mis-match factor measured at each stirrer position [4].

$$\frac{(1-|S11_{ANT}|^2)\left(1-\left|S11_{sys}\right|^2\right)}{\left|1-S11_{ANT}S11_{sys}\right|^2}$$

If the receiver system is connected to a 50 Ω load at the same ambient temperature as the chamber the $S11_{sys}$ results in a second mis-match factor.

$$\left(1-\left|S11_{sys}\right|^2\right)$$

The apparent antenna noise temperature for the antenna in the reverberation chamber is postulated in [2] to be the ambient temperature multiplied by a mis-match correction C, the ratio of the two mis-match factors at each stirrer position.

$$C = \frac{(1-|S11_{ANT}|^2)}{\left|1-S11_{ANT}S11_{sys}\right|^2} \tag{2}$$

This is demonstrated in Fig.1 which shows the apparent antenna noise temperature measured in the York reverberation chamber and the mis-match correction ratio C for each of 400 stirrer positions over one rotation of the stirrer. The measurements were made at a frequency of 800 MHz in a resolution bandwidth of 10 kHz at an ambient temperature of 301 K. The best fit line passes through 301 K at the C value of unity. The Pearson correlation coefficient of the measured data with the postulation is 0.96.

It can be seen in Fig. 1 that at some stirrer positions the apparent antenna noise temperature is above the ambient temperature. This is due to the antenna presenting a better conjugate impedance match to the receiver than the impedance match of the 50 Ω load to the receiver.

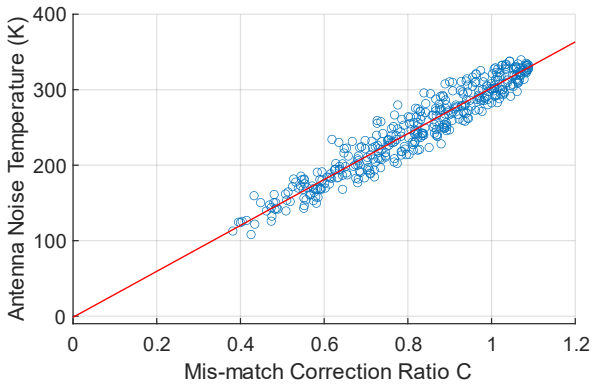

Fig. 1. Measured apparent antenna noise temperature against mis-match correction ratio C for an ambient temperature of 301 K.

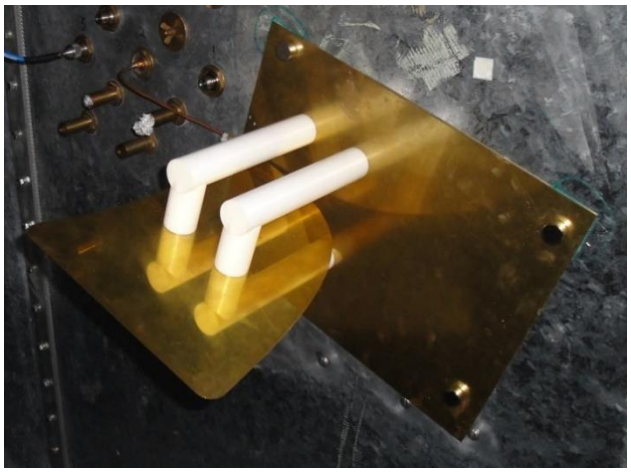

Fig. 2. Measurement antenna on the reverberation chamber wall.

In Fig. 2 shows the measurement antenna installed on the reverberation chamber wall with a semi-rigid cable leading to a coaxial penetration port in the chamber wall. The chamber has dimensions 4.7 m x 3 m x 2.4 m.

III. Signal to Noise Ratio Measurement System

The receiving system used in these experiments comprises a pre-amplifier consisting of two cascaded Mini-Circuits ZX60-1215LN amplifiers. These amplifiers have a specified maximum Noise Figure of 0.4 dB (equivalent to a maximum input noise temperature of 28 K) and the pair has an overall gain of 34 dB at 800 MHz. This is followed by an HP8447D intermediate amplifier with a gain of 26 dB and a Noise Figure of 8 dB. An Agilent EXA Signal Analyser is used as the receiver. The overall system input noise temperature, $T_{sys,}$ measured at the optimum frequency of 800 MHz at the pre-amplifier input port using a HP8970B Noise Figure Meter is 34 K (0.48 dB Noise Figure). Fig. 3 shows the packaged pre-amplifier connected to the measurement antenna coaxial penetration port on the external chamber wall. See Fig. 2 above.

Fig. 3. Packaged pre-amplifier comprising two cascaded Mini-Circuits ZX60-1215LN amplifiers.

Fig. 4. Shows the block diagram of the signal and noise measurement system. The VNA measurement reference plane for $S11_{ANT}$ and $S11_{sys}$ described in Section II above is at the coaxial port shown on the chamber wall in Fig.3.

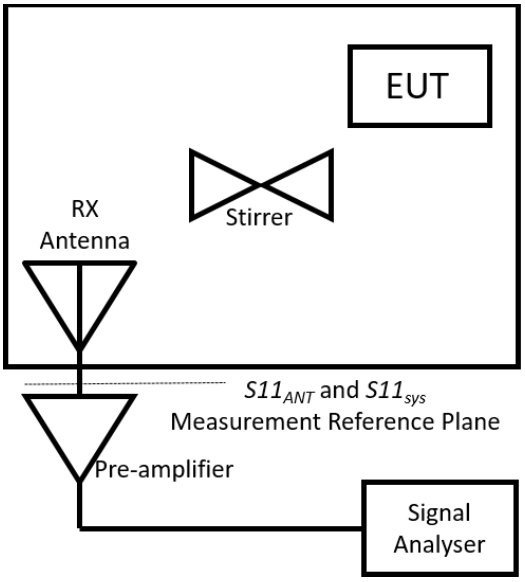

Fig. 4. Block diagram of the signal and noise power measurement system.

The simulated EUT used in these measurements comprises a metal equipment enclosure with dimensions 470 mm x 430 mm x 180 mm. The enclosure is loaded with four resistively loaded circuit cards described in [5] to simulate the enclosure contents. A dipole antenna fed by an external coaxial cable radiates into the enclosure to provide the radiated signal by leakage from the enclosure apertures and seams. Fig. 5 shows an image of the enclosure with the lid removed.

The EUT is placed on a polystyrene block in the working volume of the reverberation chamber as shown in Fig.6. Note the metre rule to the left of the EUT on the polystyrene block which is used for positioning the EUT as described in Section IV below.

The signal to noise ratio (SNR) is measured by measuring the total received noise power without the EUT signal present at each of the stirrer positions. The EUT signal is then turned on and the received signal power is measured at the same set of stirrer positions.

Fig. 5. Image of the simulated EUT showing circuit cards and the internal dipole antenna situated between the resistively loaded circuit cards.

The noise power is the amplified sum of the antenna noise power as in (1) modified by the mis-match correction ratio from (2) and the equivalent input noise power of the receiving system P_{sys}.

$$P_{sys} = kT_{sys}B \tag{3}$$

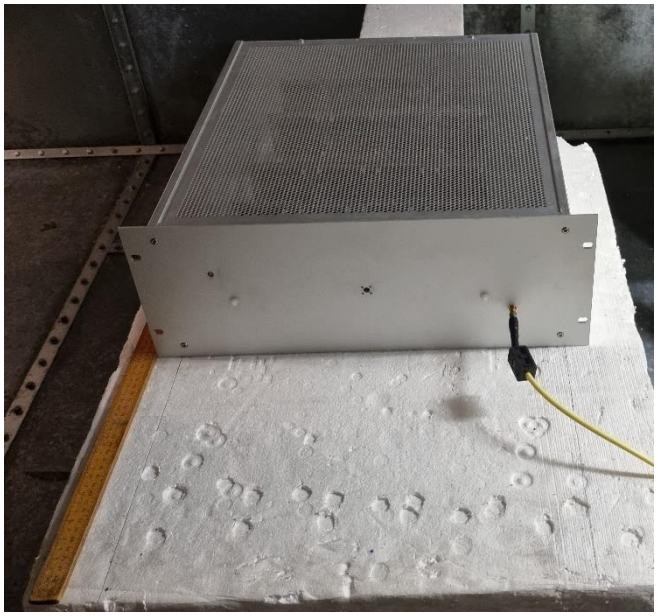

Fig.6. The assembled EUT positioned in the reverberation chamber. The external feed cable to the internal antenna is visible.

The total noise power is dominated by the antenna thermal noise power contribution from the reverberation chamber with apparent antenna noise temperatures in the range 100 K to 320 K compared to the system noise temperature of 34 K.

IV. Signal to Noise Ratio Measurement Results

The measurements presented in this section are taken at a set of six EUT positions in the working volume of the reverberation chamber. The EUT was moved along a line with measurements made at distances from the initial measurement position (0 mm) of 5 mm, 10 mm, 30 mm, 100 mm, and 300 mm.

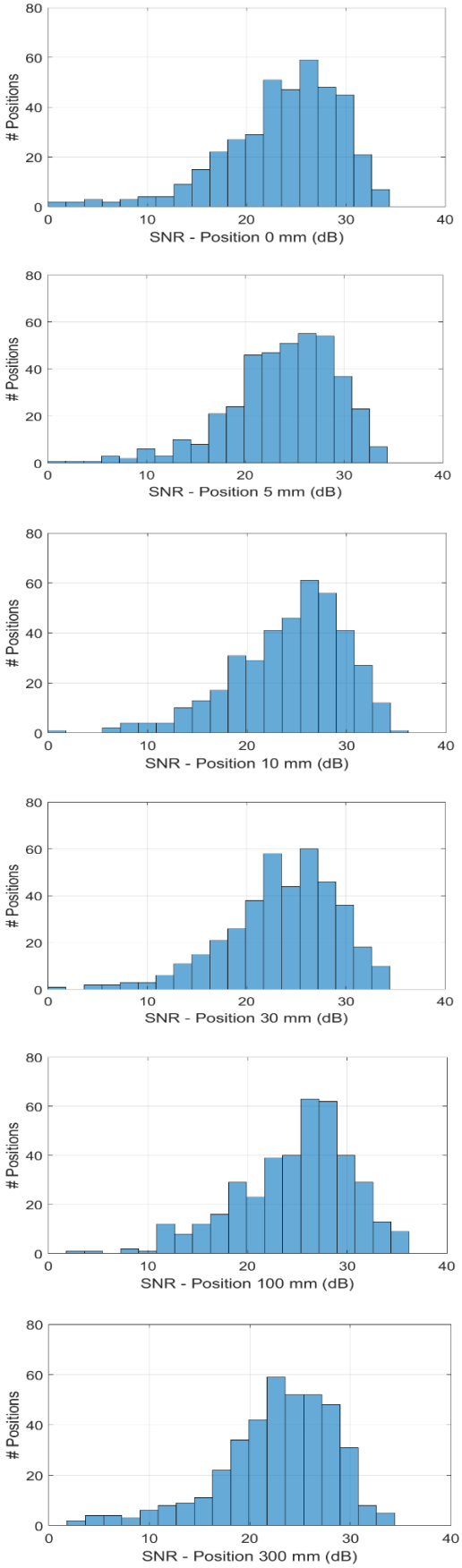

Fig. 7. Histograms showing the SNR (dB) for the six EUT measurement positions. The vertical axis, #Positions is the number of stirrer positions for each SNR bin.

For each EUT position the same set of 400 stirrer positions was used. The received signal power and the received noise power at each of the stirrer positions was recorded in order to give a SNR at each stirrer position. The measurement bandwidth of 10 kHz was chosen for speed of measurement convenience and to avoid having to compensate for the rapid variations of the frequency response of the reverberation chamber. The system exhibits the normal linear relationship between noise power and bandwidth. The EUT signal power was set to give a range of received signal powers well above the noise power so that the variability of each is easily observed.

Fig. 7 shows histograms of the observed signal to noise ratios at each of the six measurement positions. The vertical axes show the number of stirrer positions for each SNR bin. In each case the statistical distributions are comparable.

In Fig. 8 the scatter plots show the measured SNRs at each of the 400 stirrer positions for pairs of EUT positions. On each of the horizontal axes is the SNR for the reference (0 mm) position. On the vertical axes are the SNRs for displaced EUT positions of 5 mm, 10 mm, 30 mm, 100 mm, and 300 mm. As the displacement from the reference position increases, the correlation between the measured SNRs reduces. Pearson linear correlation coefficients from Fig. 8 and median SNR values for each of the measurement pairs shown from Fig. 7 are shown in Table. I. Repeat measurements with the same at the same position have a correlation coefficient of 0.9 or greater.

TABLE I.

EUT displacement from reference position (mm)	0	5	10	30	100	300
Pearson linear correlation coefficient (Fig. 8)	≥ 0.9	0.9	0.73	0.48	0.17	0.01
Median SNR (dB) (Fig. 7)	24.7	24.3	25.3	24.2	25.9	23.4

Whilst the linear correlation decreases between the signal-to-noise ratio pairs as the displacement between them increases it should be noted that the higher correlation within the scatter plot for each pair coincides with the higher values of SNR. At lower SNRs the differences at individual stirrer positions are much greater. For example, in the scatter plot in Fig. 8 showing the comparison between the reference position and the smallest 5 mm displacement where the linear correlation is highest there are stirrer positions where the difference between the two SNRs approaches 20 dB. At the larger displacements where the linear correlation is lowest the large differences in SNR can be observed at stirrer positions where one of the signal-to-noise ratios is highest. For example, on the scatter plot for the 300 mm displacement there is a stirrer position where the EUT reference position signal-to-

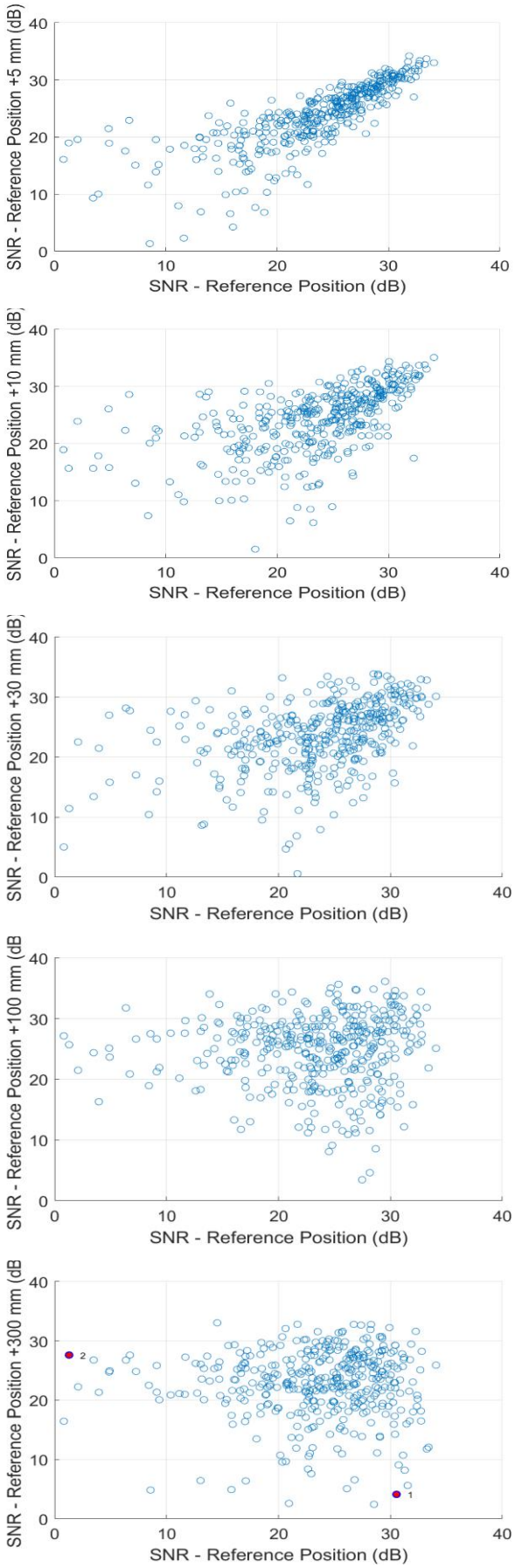

Fig. 8. Scatter plots showing the measured SNRs for the reference EUT position (0 mm) and the five other EUT positions.

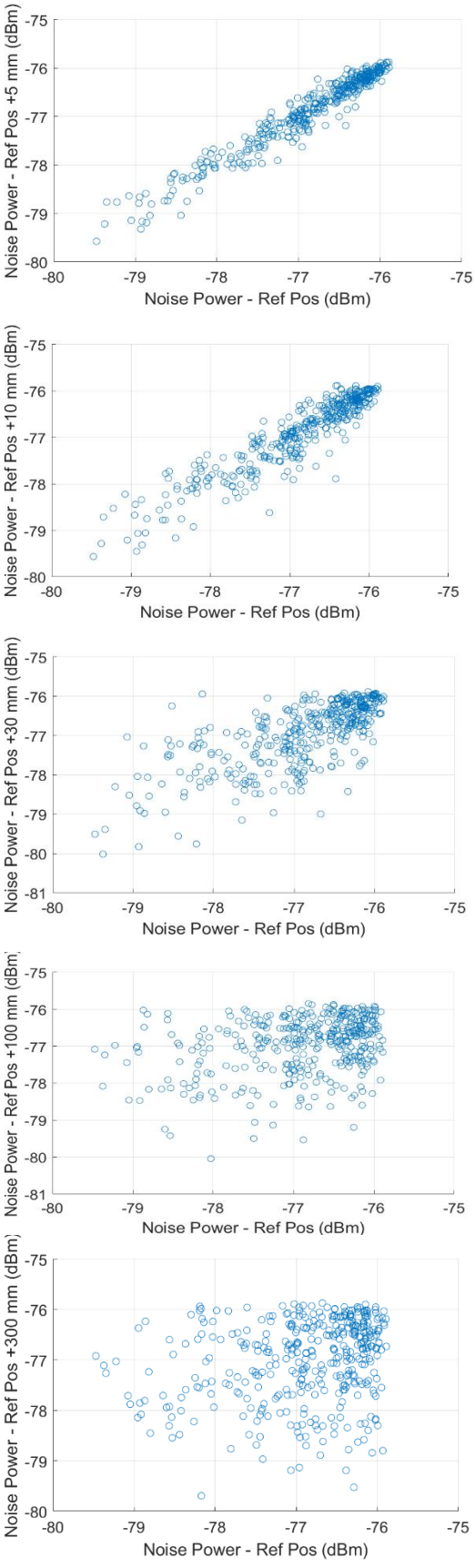

Fig. 9. Scatter plots showing the total received noise power at the signal analyser input for the reference EUT position (0 mm) and the five displaced EUT positions.

noise ratio is 31 dB and the corresponding 300 mm EUT displacement SNR is 4 dB (point 1 in Fig.8). Similarly on the same scatter plot there is a stirrer position where the 300 mm EUT displacement SNR is 28 dB and the corresponding EUT reference position SNR is 2 dB (point 2 in Fig.8).

Whilst it is accepted that the signal power at each stirrer position depends on the location of the EUT within the chamber, the behaviour of the noise power is not so obvious. In Fig. 9 scatter plots comparing the total received noise power referred to the signal analyser input port (see Fig. 4) for the reference position (horizontal axis) and at each of the five displaced positions (vertical axis) are shown for each of the four hundred stirrer positions. The level of correlation declines as it does for the SNRs of Fig. 8. However, the spread of the scatter at low noise power levels does not mirror that of the SNR scatter in Fig. 8 at low SNR values. This includes effects of the variability with stirrer position of the received signal power as well as that of the received noise power. The changes in received noise power with EUT displacement arise from the associated changes to the antenna input reflection coefficient (*S11*) effecting the mis-match correction ratio *C*.

The signal power in these measurements was set at a sufficiently high level to demonstrate SNRs significantly above one, i.e., positive dB values. For lower signal powers significant numbers of stirrer positions would show measurable signals at some stirrer positions and only noise at others. The stirrer positions where the signals are measurable would be different for each EUT position in the chamber.

V. Conclusions

In this paper the effect of thermal noise on the SNR of a signal radiated from an EUT into a reverberation chamber has been demonstrated. The SNR is determined by both the received signal level and the received noise level. The received signal level depends on the position of the EUT in the reverberation chamber and also on the position of the stirrer. The received noise level depends on the noise performance of the receiving system and on the noise temperature of the receiving antenna in the reverberation chamber. In the case of a low noise receiving system the received noise level is dominated by the apparent antenna noise temperature which is the ambient temperature of the chamber structure modified by the mis-match correction ratio as shown in [2] which is also dependent on the stirrer position and the position of the EUT. For different positions of the EUT the distribution of observed SNR values over all stirrer positions follows the same statistical distribution. However, the individual SNR values at each stirrer position vary between each EUT position.

If low signal levels are to be measured in a reverberation chamber the effects demonstrated in this paper need to be accounted for. There are clear optimum stirrer positions that enhance the strength of a weak signal relative to other stirrer positions. These optimum stirrer positions are dependent on the position of the EUT in the chamber. They are not readily predictable and measurement repeatability requires careful replication of the original EUT and chamber set-up.

Acknowledgement

Professor Emeritus Marvin is supported in this work by the Leverhulme Emeritus Fellowship EM-2021-039/4.

REFERENCES

[1] International Electrotechnical Commission, 61000-4-21 ELECTROMAGNETIC COMPATIBILITY (EMC), Part 4: Testing and Measurement Techniques, Section 21: Reverberation Chamber Test Methods. 2011.

[2] A. C. Marvin & S.J. Bale. “Thermal Noise Measurements in a Reverberation Chamber” in press in IEEE Transactions on Electromagnetic Compatibility

[3] David Hill & Mark Ma. “Aperture excitation of electrically large lossy cavities” in IEEE Transactions on Electromagnetic Compatibility, vol 36, no 3, August 1994, pp 169-177

[4] D. M. Pozar Microwave Engineering, 2nd ed., John Wiley & Sons. New York. 1998. pp 608.

[5] Ian D. Flintoft, Simon J. Bale, Andrew C. Marvin, MingYe, John F. Dawson, Changyong Wan, Mengze Zhang, Sarah L. Parker, and Martin P. Robinson. “Representative Contents Design for Shielding